Energy Engineering

Tech Science Press

DOI: 10.32604/ee.2023.028327

ARTICLE

A Temporary Frequency Response Strategy Using a Voltage Source-Based Permanent Magnet Synchronous Generator and Energy Storage Systems

Baogang Chen[1], Fenglin Miao[2,*], Jing Yang[1], Chen Qi[2] and Wenyan Ji[1]

[1]CSIC HaiZhuang Windpower Co., Ltd., Chongqing, 400000, China

[2]State Key Laboratory of Operation and Control of Renewable Energy & Storage Systems, China Electric Power Research Institute, Beijing, 100000, China

[*]Corresponding Author: Fenglin Miao. Email: a06617012@126.com

Received: 12 December 2022 Accepted: 27 April 2023 Published: 25 January 2024

ABSTRACT

Energy storage systems (ESS) and permanent magnet synchronous generators (PMSG) are speculated to be able to exhibit frequency regulation capabilities by adding differential and proportional control loops with different control objectives. The available PMSG kinetic energy and charging/discharging capacities of the ESS were restricted. To improve the inertia response and frequency control capability, we propose a short-term frequency support strategy for the ESS and PMSG. To this end, the weights were embedded in the control loops to adjust the participation of the differential and proportional controls based on the system frequency excursion. The effectiveness of the proposed control strategy was verified using PSCAD/EMTDC. The simulations revealed that the proposed strategy could improve the maximum rate of change of the frequency nadir and maximum frequency excursion. Therefore, it provides a promising solution of ancillary services for frequency regulation of PMSG and ESS.

KEYWORDS

Inertial control; PMSG; ESS; wind power generation; frequency support

1 Introduction

Due to its inexhaustible, pollution-free, and renewable nature, wind energy has been developed over the past few decades as one of the primary sources of energy worldwide. Numerous technical reports have recommended many countries set targets to satisfy their ever-growing energy demands using renewable resources and reduce carbon emissions by 2030 [1].

The increasing integration of wind energy brings significant challenges to the stability of the system frequency as the power converter-interfaced paramagnet machine synchronous generators (PMSGs; type 4 wind turbine generators) decouple the rotor speed from the system frequency [2,3]. In addition, PMSGs normally operate in the maximum power tracking mode, which would result in a reduction of the system inertia and primary frequency response [4,5]. Hence, both maximum frequency deviation and rate of change (df/dt) decrease, which may increase the possibility of inducing load-shedding relays [6,7]. The stable operating range of the PMSG rotor speed is much wider than that of the synchronous generator, and hence, the PMSG, which implements inertial control, is an effective way to control the frequency as well [8].

At present, most studies on PMSG adopt the phase-locked loop (PLL) to orientate with the power grid, e.g., system frequency, to realize power or frequency regulation by controlling the injected current [9]. This strategy is known as the current-source-control based PMSG, which displays the current-source characteristics. Based on such a PMSG strategy, df/dt [10,11] and frequency deviation (Δf) [12,13] based inertial control strategies have been developed. In references [14,15], The former aims to improve df/dt whereas the latter focuses on improving the maximum frequency deviation. Both schemes are control gain-dependent, and have been analyzed for various constant control coefficients. In addition, both df/dt and Δf based inertial control strategies are switched according to the increasing frequency deviation to improve the support stability [16].

With the increasing impedance of the grid, these phenomena would lead to abnormal interactions between the current-control-loop and PLL, resulting in instabilities [17]. Hence, the current-source-control based PMSG strategy only weakly adapts PMSG for practical implementation [18]. By imitating the dynamics of the traditional synchronous generator (TSG), the virtual synchronous generator strategy [19] and power synchronization strategy [20] emulate TSG motion dynamics, which could be denoted as the voltage source control. However, this strategy presents several limitations of PMSG implementation due to random, intermittent, and fluctuating wind generation [21]. The voltage source control directly regulates the phase and amplitude of the converter output voltage and achieves autonomous grid-synchronization without PLL [21].

In conclusion, many researches focus on designing the control strategy for frequency regulation. Both df/dt and Δf control loops with fixed control gain are implemented. Furthermore, df/dt and Δf control loops are switched when the frequency deviation reaches to a certain value. The contribution to improving the frequency support capability is limited.

The contributions of this study are summarized as follows: (1) The system frequency response model was addressed considering the frequency regulation of the PMSG and energy storage system (ESS) and the mechanisms for the same were analyzed; (2) The PMSG inertial control strategy without PLL was established. To improve the maximum df/dt and Δf, the weights in the control loops adjust the participation of the differential and proportional control based on the Δf trajectory.

This paper is organized as follows. Section 2 introduces the control of PMSG and ESS. Section 3 provides the motion features between synchronous generator and grid-side-converter of PMSG. The proposed short-term frequency regulation control strategy of PMSG and ESS is introduced in Section 4. Section 5 verifies the effectiveness of the proposed frequency regulation strategy. Section 6 draws the conclusion and illustrates the future research.

2 PMSG and ESS Control

Fig. 1 displays the PMSG structure embedded with the ESS. The mechanical power of the wind turbine can be defined as a nonlinear function, expressed as Eq. (1).

$$P_m = 0.5\rho\pi R^2 v_w^3 c_P(\lambda,\ \beta), \tag{1}$$

where ρ is the air density, R is the rotor radius, v_w is the wind speed, β is the pitch angle, λ is the tip-speed ratio, and c_p is the power coefficient expressed as Eqs. (2)–(4).

$$c_P(\lambda, \beta) = 0.645\left\{0.00912\lambda + \frac{-5 - 0.4(2.5 + \beta) + 116\lambda_i}{e^{21\lambda_i}}\right\}, \tag{2}$$

where

$$\lambda_i = \frac{1}{\lambda + 0.08\,(2.5 + \beta)} - \frac{0.035}{1 + (2.5 + \beta)^3} \tag{3}$$

and

$$\lambda = \frac{\omega_r R}{v_w}. \tag{4}$$

In Eq. (1), c_p has a maximum value, $c_{p,\max}$, at the optimal tip-speed ratio, λ_{opt}, where the PMSG is capable of capturing the maximum wind power. Substituting Eq. (4) into Eq. (1), the expression of the power reference for the maximum power tracking operation (MPTO), P_{MPPT}, can be written as

$$P_{MPPT} = 0.5\rho\pi R^2 \left(\frac{\omega_r R}{\lambda_{opt}}\right)^3 c_{p,\max} = k_g \omega_r^3, \tag{5}$$

where k_g is the coefficient for the MPPT operation of the PMSG.

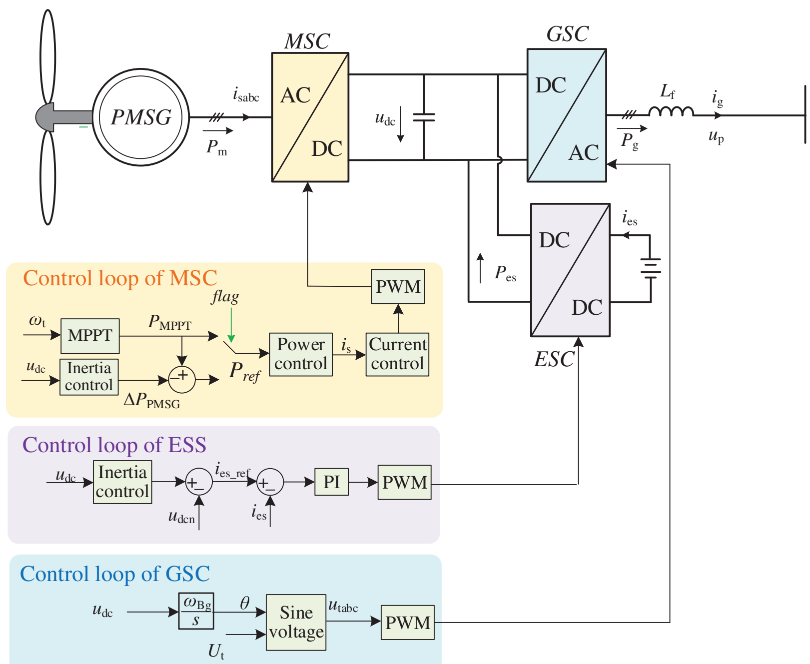

Figure 1: Control structure of the PMSG embed with ESS

The machine-side converter of the PMSG employed the vector control according to the flux linkage orientation. The MPTO was achieved based on the outer-power-control and inner-current-control loops (Fig. 1). The input of the MPTO was the rotor speed of the wind turbine. In addition, similar to the conventional PLL-based PMSG, the inertia control loop and/or other control strategies could be added to the MPTO control loops.

To achieve autonomous grid-synchronizing inertia support strategy for the PMSG, the identical relationship between the angular speed ω_s of the voltage of GSC and the DC-link voltage (u_{dc}) is established. As shown in the control loop of GSC, u_{dc} passes through an integrator with the gain of the base value of gird angular frequency, and the phase of the voltage of the GSC (θ) is the output. The reactive power is adjusted through the voltage amplitude of the GSC (u_t).

The energy storage system converter can provide frequency regulation function by absorbing or releasing energy from or to the grid. In Fig. 1, a bidirectional Buck/Boost converter is used to represent the energy storage system converter. As in the control loop, the droop control, which corresponds to the difference between the rated voltage of DC-link (u_{dcn}) and the measured value of DC-link (u_{dc}) and differential control, which corresponds to the rate of change of u_{dc} control are implemented in the energy storage system converter. Since the DC-link voltage of the PMSG decouples to the dynamics of the system frequency, the droop control and differential control could respond to the dynamics of the system frequency.

3 Motion Features between the Synchronous Generator and Grid-Side-Converter of the PMSG

The swing equation of the synchronous generator can be expressed as [19]

$$2H_{sys} \times \omega_s \times \frac{d\omega_s}{dt} = P_M - P_e, \tag{6}$$

where H_{sys} is the inertia constant of the power system; ω_s is the synchronous angular speed; and P_M and P_e are the mechanical and electrical power of the synchronous generator, respectively. Further, the dynamics of the DC-link voltage, could be expressed as

$$2H_C\left(u_{dcn}\frac{du_{dc}}{dt}\right) = P_m - P_g, \tag{7}$$

where u_{dcn} is the nominal voltage of the DC-link; u_{dc} is the measured voltage of the DC-link; P_m and P_g are the mechanical and electrical power of the PMSG, respectively, and H_C is the inertia constant of the capacitor defined as

$$H_C = \frac{Cu_{dcn}^2}{2S_n}, \tag{8}$$

where C is the capacitance and S_n is the apparent power of the PMSG. The DC-link voltage of the PMSG has a similar dynamic motion equation to that of the synchronous generator (Fig. 2). It displays the analogous dynamic features to Hsys [20].

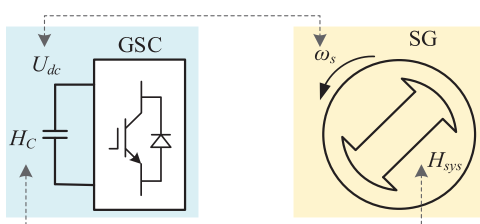

Figure 2: Motion feature similarity between the grid side converter and synchronous generator

4 Short-Term Frequency Regulation Control Strategy for PMSG and ESS

Figs. 3a and 3b display the structures of the PMSG and ESS inertial control strategy, respectively.

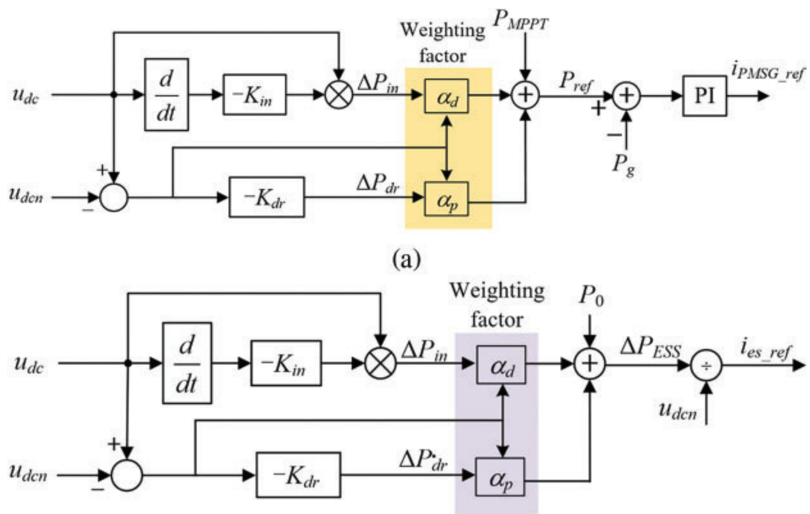

Figure 3: Structure of the inertial control scheme for PMSG and ESS. (a) Structure of the inertial control scheme for PMSG; (b) Structure of the inertial control scheme for ESS

The additional power from the PMSG and ESS can be calculated based on the outputs of the du_{dc}/dt control loop (ΔP_{in}, top loop), Δu_{dc} control loop (ΔP_{dr}, bottom loop) and the power reference of MPPT control (P_{MPPT}), as in Eqs. (9) and (10).

$$\Delta P_{in} = -K_{in} \cdot u_{dc} \cdot \frac{du_{dc}}{dt}, \tag{9}$$

$$\Delta P_{dr} = -K_{droop}(u_{dc} - u_{dcn}) = -K_{droop} \cdot \Delta u_{dc}, \tag{10}$$

where K_{in} and K_{droop} indicate the control gains for the $d\Delta u_{dc}/dt$ and Δu_{dc} control loops, respectively.

Prior to a frequency disturbance, we have $P_{ref} = P_{MPPT}$. After a disturbance, the additional power (Eqs. (9) and (10)) from the PMSG inertial control, which is dependent on the measured voltage of the DC-link, was added to P_{MPPT} (Fig. 3a; Eq. (11)). Furthermore, the same ΔP_{in} and ΔP_{dr} were calculated and added also to the ESS control loop. The P_{ref} value is used to calculate the current of the MSC by dividing it by the DC voltage; it can be expressed as

$$P_{ref} = P_{MPPT} + \Delta P_{dr} + \Delta P_{in}, \tag{11}$$

$$P_{ref} = P_0 + \Delta P_{dr} + \Delta P_{in}, \tag{12}$$

where P_0 is the ESS initial output power. The instantaneous frequency excursion ($\Delta f(t)$) can then be derived using the low-order system frequency response model [22] as

$$\Delta f(t) = \frac{\Delta P}{K_1 + D}\left[1 + \alpha e^{-\xi\omega_n t} \sin(\omega_d t + \beta)\right], \tag{13}$$

where

$$\omega_n = \sqrt{\frac{DR + K_m}{2HRT_R}}, \tag{14}$$

and

$$\xi = \left(\frac{2HR + (DR + K_{\mathrm{m}}F_{\mathrm{H}})\,T_{\mathrm{R}}}{2\,(DR + K\mathrm{m})}\right)\omega_{\mathrm{n}}, \tag{15}$$

where ω_n is the natural oscillation frequency; ξ is the damping ratio; ω_d is the damped frequency; α and β are the coefficients derived from the model; and ΔP is the equivalent size of the frequency disturbance. The maximum frequency excursion can be represented as [22]

$$\Delta f_{\max} = \frac{\Delta P}{K_1 + D}\left(1 + \alpha_1 e^{-\xi\omega_{\mathrm{n}} t_{\mathrm{nadir}}}\right), \tag{16}$$

where K_1 is the setting value of the primary governor response and ΔP_{RE} is the sum of the PMSG and ESS additional powers.

Similar to reference [15], the system frequency response model performance improved (Fig. 4). The equivalent size of the disturbance (ΔP) was calculated as

$$\Delta P = \Delta P_{\mathrm{L}} - \Delta P_{\mathrm{RE}} = \Delta P_{\mathrm{L}} - (\Delta P_{PMSG} + \Delta P_{ESS}), \tag{17}$$

where ΔP_{PMSG} and ΔP_{ESS} represent the additional powers generated from the PMSG and ESS when performing the short-term frequency support.

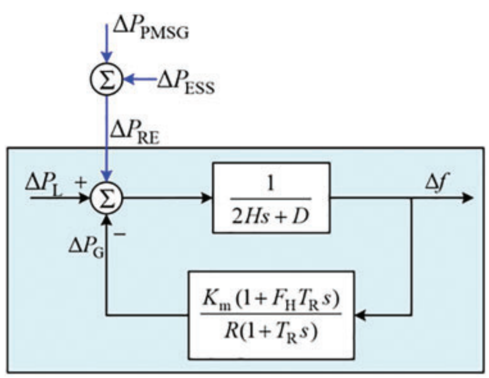

Figure 4: System frequency response considering frequency regulation of PMSG and ESS

The maximum frequency excursion can be derived as [22]

$$\Delta f_{\max} = \frac{\Delta P_{\mathrm{L}} - \Delta P_{\mathrm{RE}}}{K_1 + D}\left(1 + \alpha_1 e^{-\xi\omega_{\mathrm{n}} t_{\mathrm{nadir}}}\right) \tag{18}$$

In Eq. (18), the PMSG and ESS could support the system frequency. With the larger ΔP_{RE}, the molecule of Eq. (18) decreases so that the maximum frequency excursion could be enhanced. For the voltage source control based on the inertial synchronization strategy (without PLL), u_{dc} in p.u. is the same as the system frequency in p.u. Therefore, Eqs. (9) and (10) can be rewritten as

$$\Delta P_{in} = -K_{in}\cdot U_{\mathrm{dc}}\cdot\frac{dU_{\mathrm{dc}}}{dt}, \tag{19}$$

$$\Delta P_{dr} = -K_{droop}\,(U_{\mathrm{dc}} - U_{\mathrm{dcn}}) = -K_{droop}\cdot\Delta U_{\mathrm{dc}}. \tag{20}$$

Fig. 5 illustrates the system frequency trajectory after an under-frequency-disturbance. This trajectory can be divided into Zone 1 corresponding to a large df_{sys}/dt, Zone 2 corresponding to a large

Δf_{sys}, and Zone 3 corresponding to frequency rebounding. During the initial period, ΔP_{in} and ΔP_{dr} were dominant around the maximum frequency deviation (Fig. 5). Since (i) the objective of the df/dt and Δf control loops are different and (ii) the available PMSG kinetic energy and charging/discharging capacities are restricted, to improve df_{sys}/dt and Δf_{sys}, ΔP_{in} and ΔP_{dr} were adjusted according to the instantaneous system frequency-based weights (α_p for ΔP_{dr} and α_d for ΔP_{in}) as (Fig. 3)

$$\Delta P = \alpha_d \Delta P_{\text{in}} + \alpha_p P_{\text{dr}}. \tag{21}$$

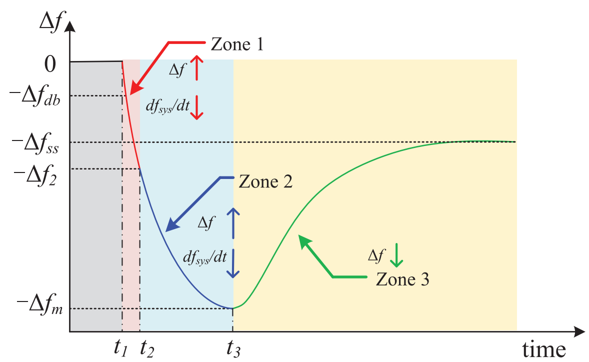

Figure 5: System frequency trajectory following an under-frequency-disturbance

These weights regulate the participation of the df_{sys}/dt and Δf_{sys} control loops to effectively maximize df_{sys}/dt and Δf_{sys} (in this manuscript, Δf_{sys} and df_{sys}/dt are equivalent to ΔU_{dc} and dU_{dc}/dt, respectively).

The objective of categorizing the frequency trajectory into the three zones is described as follows:

- Zone 1: To improve df_{sys}/dt, its control loop must be undervalued. Therefore, α_d gradually decreases from a value of 2 and α_p increases from a value of 0 (Fig. 6a). The trajectory moves from the right-hand side to the left-hand side with increasing frequency deviation. Parameters α_d and α_p for Zone 1 are expressed as

$$\begin{cases} \alpha_d = 2e^{12\Delta f} \\ \alpha_p = 2\left(1 - e^{12\Delta f}\right) \end{cases}. \tag{22}$$

- Zone 2: PMSG and ESS focus on improving the frequency nadir by undervaluing the Δf_{sys} control loop. Therefore, α_d decreases to 0 and α_p increases to 1 (Fig. 6b). The trajectory moves from the right-hand side to the left-hand side as the increasing Δf_{sys}. Parameters α_d and $\alpha_p$for Zone 2 are expressed as

$$\begin{cases} \alpha_d = \dfrac{2}{1 + e^{-40(\Delta f + 0.057)}} \\ \alpha_p = 2 - \dfrac{2}{1 + e^{-40(\Delta f + 0.057)}} \end{cases}. \tag{23}$$

- Zone 3: The system frequency rebounds in this region. Here, $\alpha_d = 0$ to avoid the negative impact of the df_{sys}/dt control loop and we fix $\alpha_p = 1$.

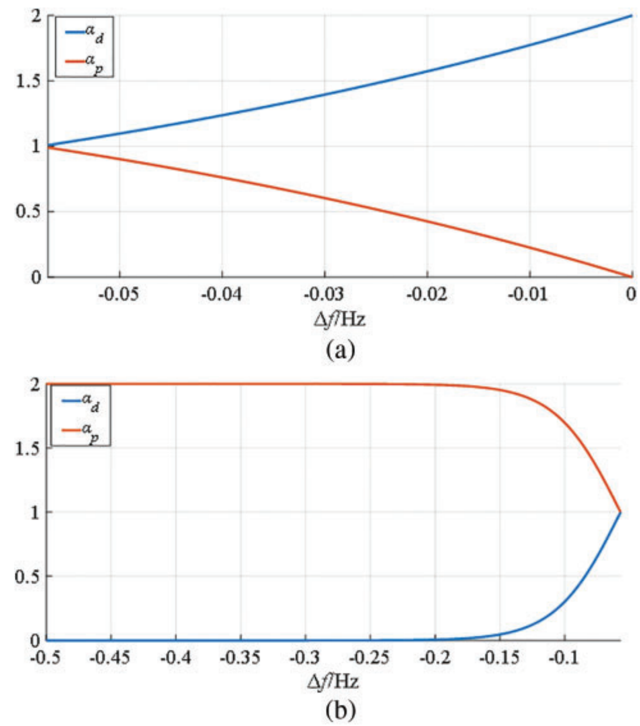

Figure 6: Features of weighting factors: (a) Weighting factor for Zone 1; (b) Weighting factor for Zone 2

5 Simulation Verification

To verify the effectiveness of the suggested frequency support strategy, a simulation model system consisting of the PMSG embedded with ESS, one synchronous generator, and two local loads (L_1 and L_2), is built on the PSCAD/EMTDC, as illustrated in Fig. 7. The parameters of PMSG and synchronous generator are represented in Tables 1 and 2. The ratings of synchronous generator and PMSG are 3 MVA and 2 MVA, respectively. L_1 is the static load as 4.0 MW and L_2 is the dump load as 0.4 MW. In the governor system of synchronous generator, the droop setting is set to 4%. For the conventional short-term frequency regulation, K_{in} and K_{droop} are set to 20. Δf_{db} and Δf_2 are set to 0.02 Hz [20] and 0.2 Hz, respectively. Two scenarios are carried out to illustrate the effectiveness of the proposed short-term frequency support under various types of frequency disturbance.

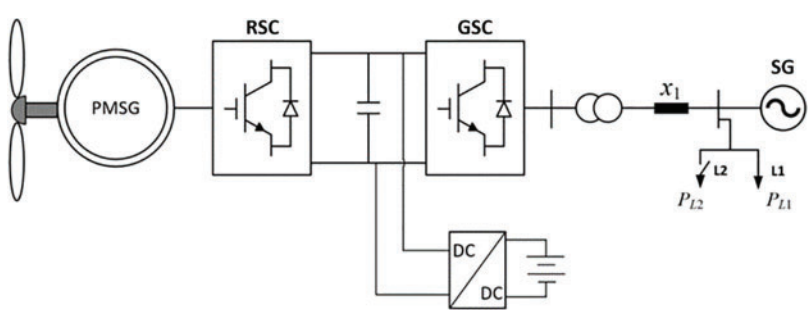

Figure 7: Outline of the test system

Table 1: Parameters of PMSG embed ESS

Symbol	Item	Value	Units
S_N	Rated power	2	MW
U_N	AC phase voltage rated value	0.563	kV
u_{dcn}	DC-link voltage rated value	1.1	kV
L_s	Synchronous inductance	0.5495	p.u.
R_s	Stator resistance	0.00387	p.u.
H_{WT}	Inertia constant	4	s
H_C	Inertia constant of DC-link capacitor	3.6	ms
U_{ESS}	Rated value of battery voltage	0.78	kV

Table 2: Parameters of synchronous generator

Symbol	Item	Value	Units
S_g	Rated capacity	3	MVA
U_g	Terminal voltage	0.69	kV
H_g	Inertia time constant	4	s
R	Droop setting	4	%
T_g	Governor time constant	8.408	s
T_d, T_d, T_q	Time constant of synchronous generator	0.635, 0.015, 0.015	s

In the simulation results, "MPPT" means no frequency regulation action from the PMSG and ESS. "VIC" means that the PMSG and ESS could provide conventional virtual inertial control strategy with the control coefficient of 10 and 20 for K_{in} and K_{droop}. "WF-VIC" means the proposed virtual inertial control strategy of PMSG and ESS with adjusting weighting factor.

5.1 Case 1: Scenario of Load Sudden Connection

Fig. 8 illustrates the simulation results of the various strategies for decreasing grid frequency. When no frequency regulation scheme (MPPT) was applied for the PMSG and ESS, the frequency nadir was 49.6 Hz (0.992 p.u.). The voltage of the DC-link decreased to $u_{dc} = 0.992$ p.u. with the same frequency trajectory, as the system frequency is coupled with the DC-link voltage. When the traditional short-term frequency regulation (VIC) with a fixed control coefficient was implemented in the PMSG and ESS, the grid frequency decreased to 49.7 Hz (0.994 p.u.). The DC-link voltage decreased to $u_{dc} = 0.994$ p.u., after the system frequency was increased slightly above that of "MPPT" (Figs. 8a and 8c).

The frequency nadir of the suggested frequency regulation strategy is improved to 0.995 p.u. (49.731 Hz) as well as the voltage of DC-link. In addition, the maximum frequency rate of change (df/dt) for the suggested frequency regulation strategy is 0.0043 p.u./s, which is less than the conventional strategy due to the rapid power injection, as shown in Fig. 8b.

The maximum power injection of the PMSG for the suggested frequency regulation is 0.214 p.u. which is more than that of the conventional scheme by 0.084 p.u., as shown in Fig. 8d. In addition, the same amount of power is injected from the ESS in p.u. due to the same input and control coefficient. This is the reason why the suggested frequency regulation strategy could improve the maximum deviation of the system frequency and voltage of the DC-link (see Fig. 8e).

The rotor speed nadir of the suggested frequency regulation strategy is 0.974 p.u., which is more than that of the conventional scheme by 0.054 p.u. As a result, more power is injected to the power grid to support the dynamic system frequency (see in Fig. 8f), the same performance would be observed in the state of change of ESS.

As shown in Fig. 8g, at the initial stage of disturbance, a_d decreases from two to zero to improve the maximum df/dt, whereas α_p increases with the increase of the frequency deviation to improve the maximum frequency excursion.

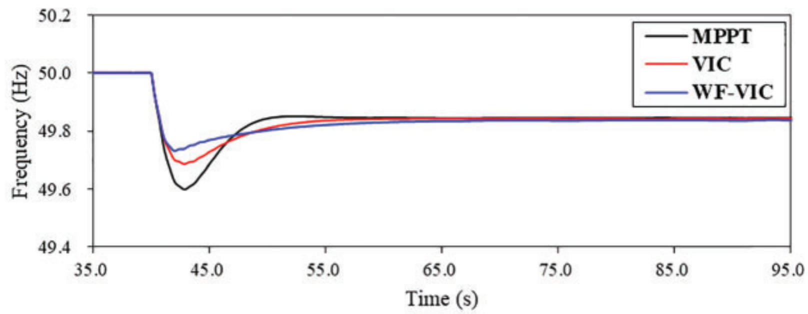

(a)

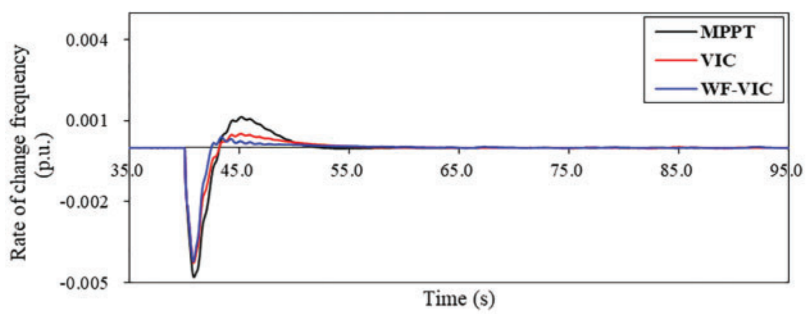

(b)

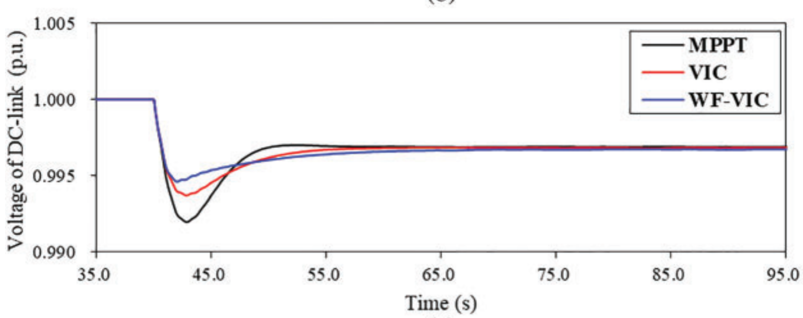

(c)

Figure 8: (Continued)

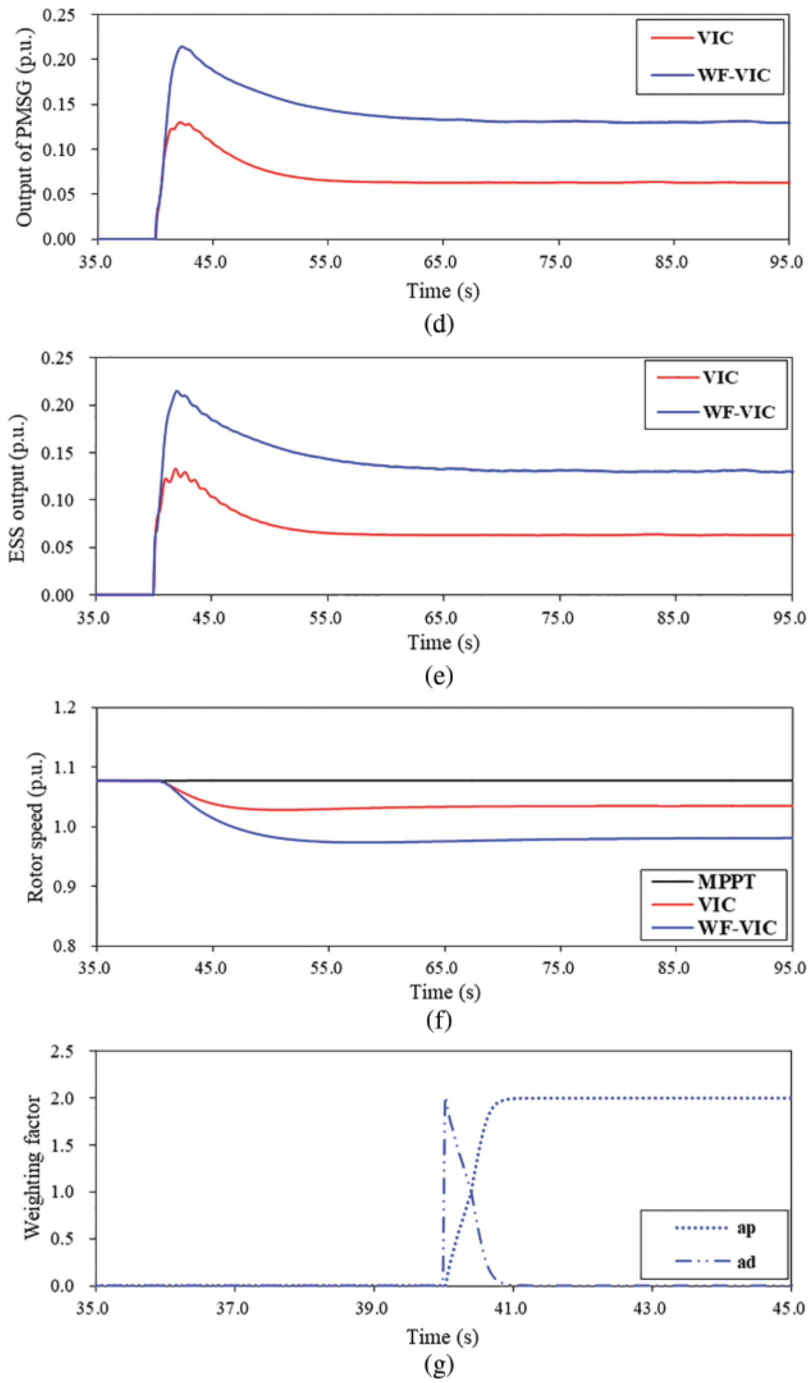

Figure 8: Simulation results: (a) System frequency; (b) Rate of change of frequency; (c) Voltage of DC-link; (d) Output of PMSG; (e) Output of ESS; (f) Rotor speed; (g) Weighting factor

5.2 *Case 2: Scenario of Load Disconnection*

Fig. 9 illustrates the simulation results when the grid frequency increases. For the case of "MPPT", the frequency nadir is 50.408 Hz (1.008 p.u.), and the voltage of DC-link increases to 1.008 p.u. with the same locus of the system frequency. If the traditional short-term frequency regulation with fixed control coefficient implements in the PMSG and ESS, the grid frequency increases to 50.322 Hz (1.006 p.u.), and the DC-link voltage u_{dc} follows the increase in grid frequency. The frequency nadir and voltage of DC-link of the suggested frequency regulation strategy are improved to 1.005 p.u. (50.278 Hz), as shown in Figs. 9a and 9c. In addition, the maximum df/dt for the suggested frequency regulation strategy is 0.0045 p.u./s, which is less than that of the conventional strategy due to the rapid power reduction, as shown in Fig. 9b. Thus, as in Case 1, the proposed scheme could improve the maximum frequency excursion and reduce the maximum.

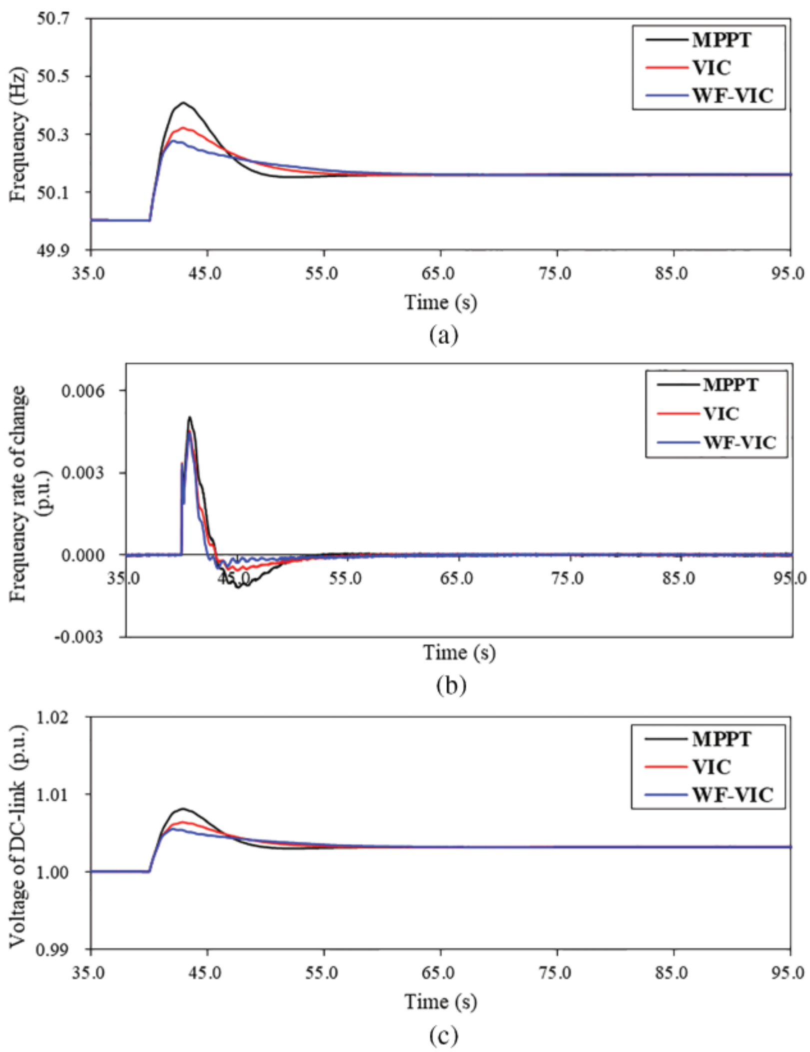

Figure 9: (Continued)

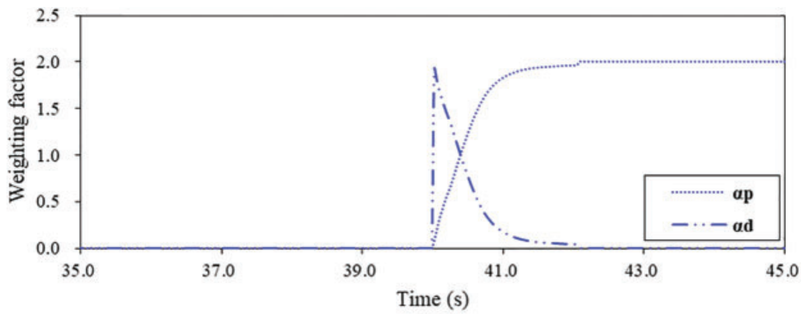

(d)

Figure 9: Simulation results: (a) System frequency; (b) Rate of change of frequency; (c) Voltage of DC-link; (d) Weighting factor

As in Case 1, a_d decreases from two to zero to improve the maximum df/dt, whereas α_p increases with the increase of the frequency deviation to store more power in the PMSG and ESS (see Fig. 9e).

6 Conclusions

High wind power penetration power system would face the problem of system frequency stability due to the power electronics interfaced PMSG. PMSG and ESS could participate in frequency regulation by adding the differential control loop and proportional control loop. Constrained by constant gain, the frequency support capability is restricted. Meanwhile, the available kinetic energy of the PMSG and charging/discharging capacity are restricted. To address the reduced frequency support capability while effectively utilizing the frequency regulation resources, the short-term frequency support of PMSG and ESS is suggested. To this end, firstly, the system frequency response model is addressed, considering the frequency regulation of the PMSG and ESS. The mechanism of the frequency regulation for the PMSG and ESS is analyzed, then the weighting factors are embedded in the control loops to adjust the participation of the differential control and proportional control based on the trajectory of system frequency excursion in the machine side converter. In grid side converter, the voltage of DC-link capacitor would automatically respond to the dynamic system frequency without employing PLL. In addition, the additional ESS with combined inertial control loops is embedded on the DC side of the PMSG to improve the frequency regulation capability further.

Simulation studies clearly verified that the suggested short-term frequency regulation of the voltage source control based on PMSG and ESS can improve the frequency nadir under various system frequency disturbances.

In future, the coordinated control between the PMSG and ESS would be designed considering the available kinetic energy of the PMSG and charging/discharging capacity. In addition, the realistic wind speed conditions would be considered to investigate the effectiveness of the proposed strategy.

Acknowledgement: None.

Funding Statement: This work was financially supported by Open Fund of National Engineering Research Center for Offshore Wind Power "Stabilization Mechanism and Control Technology of the Intelligent Wind-Storage Integration System Based on Voltage-Source and Self-Synchronizing Control (HSFD22007)".

Author Contributions: All authors contributed to the review & editing of this paper. In addition, Baogang Chen and Fenglin Miao contributed to the methodology, software, analysis.

Availability of Data and Materials: Data would be available after request.

Conflicts of Interest: The authors declare that they have no conflicts of interest to report regarding the present study.

References

1. Hajahmadi, M. A., Gharehpetian, G. B., Firouzi, M., Anvari-Moghaddam, A. (2022). Output power smoothing of wind power plants using unified inter-phase power controller equipped with super-capacitor. *Journal of Energy Storage, 54,* 105–209.
2. Yang, D., Yan, G., Zheng, T., Zhang, X., Hua, L. (2022). Fast frequency response of a DFIG based on variable power point tracking control. *IEEE Transactions on Industry Applications, 58(4),* 5127–5135.
3. Muljadi, E., Gevorgian, V., Singh, M., Santoso, S. (2012). Understanding inertial and frequency response of wind power plants. *2012 IEEE Power Electronics and Machines in Wind Applications*, pp. 1–8. IEEE.
4. Kabsha, M. M., Rather, Z. H. (2020). A new control scheme for fast frequency support from HVDC connected offshore wind farm in low-inertia system. *IEEE Transactions on Sustainable Energy, 11(3),* 1829–1837.
5. Kim, J., Mujadi, E., Gevorgian, V., Hoke, A. F. (2019). Dynamic capabilities of an energy storage-embedded PMSG system. *IEEE Transactions on Industry Applications, 55(4),* 4124–4134.
6. Eto, J. H. (2010). *Use of frequency response metrics to assess the planning and operating requirements for reliable integration of variable renewable generation*. USA: Lawrence Berkeley National Laboratory.
7. Gevorgian, V., Zhang, Y., Ela, E. (2015). Investigating the impacts of wind generation participation in interconnection frequency response. *IEEE Transactions on Sustainable Energy, 6(3),* 1004–1012.
8. Wang, S., Tomsovic, K. (2019). A novel active power control framework for wind turbine generators to improve frequency response. *IEEE Transactions Power System, 33(6),* 6579–6589.
9. Rocabert, J., Luna, A., Blaabjerg, F. (2012). Control of power converters in AC and DC microgrids. *IEEE Transactions on Power Electronics, 27(11),* 4734–4749.
10. Lorenzo, Z., Andreas, J. R., Janus, M. S., Ioannis, M., Hansen, A. D. (2013). Virtual inertia for variable speed wind turbines. *Wind Energy, 16(8),* 1225–1239.
11. Peng, X., Yao, W., Yan, C., Wen, J., Cheng, S. (2020). Two-stage variable proportion coefficient-based frequency support of grid connected PMSG-WTs. *IEEE Transactions Power System, 35(2),* 962–974.
12. Lee, J., Jang, G., Muljadi, E., Blaabjerg, F., Chen, Z. (2016). Stable short-term frequency support using adaptive gains for a PMSG-based wind power plant. *IEEE Transactions on Energy Conversion, 31(3),* 1068–1079.
13. Yang, D. J., Jin, Z. Y., Zheng, T. Y., Jin, E. S. (2022). An adaptive droop control strategy with smooth rotor speed recovery capability for type III wind turbine generators. *International Journal of Electrical Power & Energy Systems, 135,* 107532–107542.
14. Fu, Y., Wang, Y., Zhang, X. (2017). Integrated wind turbine controller with virtual inertia and primary frequency responses for grid dynamic frequency support. *IET Renewable Power Generation, 11(8),* 1129–1137.
15. Margaris, I. D., Papathanassiou, S. A., Hatziargyriou, N. D., Hansen, A. D., Sorensen, P. (2012). Frequency control in autonomous power systems with high wind power penetration. *IEEE Transactions on Sustainable Energy, 3(2),* 189–199.

16. Ma, Z. H., Li, X. R., Tan, Z. X., Huang, J., He, L. (2019). Integrated control of primary frequency regulation considering dead band of energy storage. *Transactions of China Electrotechnical Society, 34(10),* 2102–2115.
17. Zhang, C., Cai, X., Rygg, A., Molinas, M. (2018). Sequence domain SISO equivalent models of a grid-tied voltage source converter system for small-signal stability analysis. *IEEE Transactions on Energy Conversion, 33(2),* 741–749.
18. Zhu, K., Sun, P., Zhou, L., Du, X., Luo, Q. (2020). Frequency-division virtual impedance shaping control method for grid-connected inverters in a weak and distorted grid. *IEEE Transactions on Power Electronics, 35(8),* 8116–8129.
19. Zhong, Q., Weiss, G. (2011). Synchronverters: Inverters that mimic synchronous generators. *IEEE Transactions on Industrial Electronics, 58(4),* 1259–1267.
20. Zhang, L., Harnefors, L., Nee, H. P. (2010). Power-synchronization control of grid-connected voltage-source converters. *IEEE Transactions on Power Systems, 25(2),* 809–820.
21. Sang, S., Zhang, C., Cai, X., Molinas, M., Zhang, J. et al. (2019). Control of a type-IV wind turbine with the capability of robust grid-synchronization and inertial response for weak grid stable operation. *IEEE Access, 7,* 58553–58569.
22. Shi, Q., Li, F., Cui, H. (2018). Analytical method to aggregate multi-machine SFR model with applications in power system dynamics studies. *IEEE Transactions Power System, 33(6),* 6355–6367.